THE JOURNAL OF PHYSICAL CHEMISTRY B

Article

pubs.acs.org/JPCB

Molecular Dynamics Simulations to Provide New Insights into the Asymmetrical Ammonium Ion Movement Inside of the $[d(G_3T_4G_4)]_2$ G-Quadruplex DNA Structure

Parisa Akhshi, Gregory Acton, and Gang Wu*

Department of Chemistry, Queen's University, 90 Bader Lane, Kingston, Ontario, Canada K7L 3N6

Supporting Information

ABSTRACT: We have used both adaptive biasing force (ABF) and regular molecular dynamics (MD) simulations to investigate the asymmetrical NH_4^+ ion movement inside of a bimolecular G-quadruplex DNA structure $[d(G_3T_4G_4)]_2$. The free-energy landscapes obtained from ABF MD simulations suggest that the NH_4^+ ion exiting the $[d(G_3T_4G_4)]_2$ G-quadruplex stem in the direction toward the edge-type loop (denoted as the upper direction) experiences a lower free-energy barrier than that toward the diagonal loop (denoted as the lower direction) by approximately 3−4 kcal mol^{-1}. This result is in qualitative agreement with the previous discovery made by Šket and Plavec on the same G-quadruplex structure from ^{15}N NMR experiments (*J. Am. Chem. Soc.* **2007**, *129*, 8794). In the Na^+ form of the same G-quadruplex, Na^+ ion movement was found to be symmetrical, with a free-energy barrier of only 5−7 kcal mol^{-1} to cross all three G-quartets, that is, $[d(G_3T_4G_4)]_2$ still exhibits ion-channel-like behaviors for Na^+ ions. On the basis of the new computational results, we hypothesize that the stiffness of a G-quartet is primarily determined by the base stacking interactions within the G-quadruplex stem. Therefore, the structural origin for the asymmetrical NH_4^+ ion movement in $[d(G_3T_4G_4)]_2$ is the presence of two different modes of base stacking around the NH_4^+ binding sites, a more stable 5′-syn−anti mode between lower and central G-quartets and a less stable 5′-anti−anti mode between upper and central G-quartets. Simulations also suggest that loop topology at the end of a G-quadruplex stem only controls the direction at which an exiting NH_4^+ ion reaches bulk solution but does not impose significant free-energy barriers.

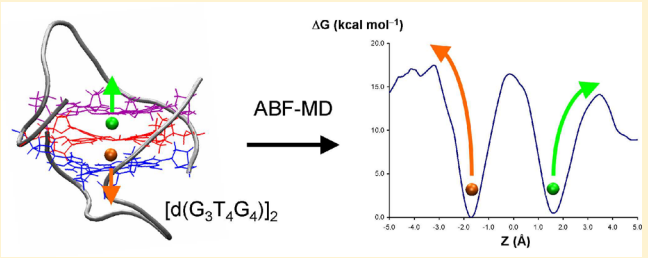

1. INTRODUCTION

DNA and RNA sequences containing guanine-rich tracts can fold into high-ordered structures known as G-quadruplexes. The basic structural motif in G-quadruplexes is a hydrogen-bonded guanine tetramer called the G-quartet. It is also well-established that formation of such G-quadruplexes requires the presence of monovalent ions such as Na^+, K^+, and NH_4^+.[1−4] Typically, these ions reside inside of the G-quadruplex stem, each being fully dehydrated and coordinated to eight carbonyl oxygen atoms from guanine bases. This special G_4−ion−G_4−ion−G_4 arrangement inside of a G-quadruplex stem is reminiscent of the situation seen in K^+ ion channel proteins, as first pointed out by Feigon and co-workers.[5] Because of this structural similarity, the stacking G-quartet motif was considered to be a candidate in the design of artificial ion channels.[6,7] While structural information and NMR spectral data about the modes of ion binding inside of G-quadruplex stems are abundant in the literature, much less is known about the energetic and dynamic properties of ion movement through a G-quadruplex DNA stem or channel. It is this latter aspect that is critical for the potential applications of G-quadruplex DNA as ion channels. As NH_4^+ ions can be readily monitored by ^{15}N and ^1H NMR, a considerable amount of information has been accumulated about NH_4^+ ion movement through G-quadruplex channels, as originally demonstrated by Feigon, Hud, and co-workers[8−10] and more recently by Plavec and co-workers.[11−17] Although other metal ions such as Na^+, K^+, Rb^+, Tl^+, and Ca^{2+} are also known to be important for G-quadruplex formation, they are much more difficult to study by spectroscopic methods than NH_4^+. As a result, only a few NMR studies can be found in the literature for direct detection of these ions in G-quadruplex DNA and related molecular systems in the solid state[18−25] and in solution.[26−33] These previous studies have shown that the ion movement in G-quadruplex DNA generally occurs on a time scale between milliseconds and seconds. As this type of long-time scale or very slow ion movement is always associated with steep features in the free-energy landscape, it is rather difficult to achieve satisfactory sampling in the configuration space by classic brute-force molecular dynamics (MD) simulations. Nonetheless, we should note that both conventional MD simulations[34−45] and quantum chemical calculations[46−53] have been previously used to generate useful information about various aspects of G-quadruplex DNA structure and dynamics.

Received: May 16, 2012
Revised: July 10, 2012
Published: July 10, 2012

   dx.doi.org/10.1021/jp304760k | *J. Phys. Chem. B* 2012, 116, 9363−9370

In a recent study,[54] we established for the first time the validity of adaptive biasing force (ABF) MD simulations[55−60] in evaluating free-energy landscapes for ion movement (Na^+, K^+, and NH_4^+) in G-quadruplex DNA structures. Here, we apply this computational method to investigate the NH_4^+ ion movement inside of a bimolecular G-quadruplex DNA structure formed by $d(G_3T_4G_4)$, denoted as $[d(G_3T_4G_4)]_2$. As shown in Figure 1, this G-quadruplex structure consists of a three G-quartet stem, one edge-type and one diagonal loop.[12] Inside of the stem, two NH_4^+ ions are present. A few years ago, Šket and Plavec[13] observed that the two bound NH_4^+ ions exit the stem in a distinctly asymmetrical fashion. In particular, they found that the NH_4^+ ion transport rate is 10 times faster for the "upper" NH_4^+ ion than that for the "lower" NH_4^+ ion. This was the first case that ion movement through a G-quadruplex stem is shown experimentally to be asymmetrical. In addition, they observed that the NH_4^+ ion never crosses the central G-quartet from either binding site. Thus, they concluded that this particular G-quadruplex DNA does not exhibit ion-channel-like properties for NH_4^+. In this context, a fundamental question should be asked about the structural basis for such an asymmetrical ion movement. Furthermore, is there any general principle that allows one to predict whether a particular G-quadruplex fold may or may not exhibit ion-channel-like properties? As there are very few cases in which reliable experimental data are available with respect to ion movement in G-quadruplex DNA, we decided to use the ABF MD computational approach to gain some insights into the asymmetrical NH_4^+ ion movement in this important G-quadruplex structure. The main objectives of this study are (1) to further evaluate the accuracy of the ABF MD approach in obtaining free-energy barriers for ion movement in G-quadruplexes and (2) to apply this computational approach to examine the very unusual ion movement in $[d(G_3T_4G_4)]_2$ G-quadruplex DNA.

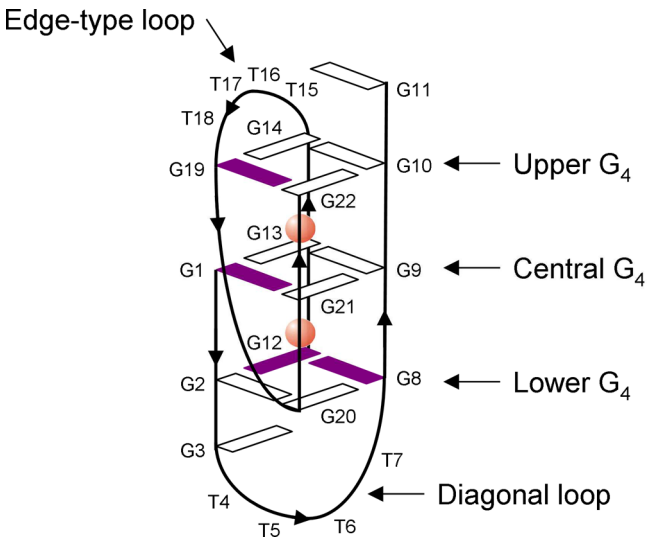

Figure 1. Schematic diagram showing the folding of the $[d(G_3T_4G_4)]_2$ G-quadruplex and the locations of two bound NH_4^+ ions (balls) inside of the G-quadruplex stem. Shaded and open rectangles are the G residues in syn and anti conformations, respectively.

2. EXPERIMENTAL SECTION

2.1. Regular MD Simulations. Solution NMR structure of $[d(G_3T_4G_4)]_2$ (PDB code 1U64)[12] was used as the initial structure. Two ions were manually added to the two-channel binding sites. All DNA systems were charge-neutralized by adding an appropriate number of counterions. Then, the systems were immersed in a box of TIP3P water molecules extending up to 10 Å from the solute in each direction. The systems were then optimized and equilibrated using multiple initial minimization and dynamics runs. A 10000-step minimization of water and counterions was carried out with solute and inner-bound ions restrained by a force constant of 500 kcal mol^{-1} $Å^{-2}$ for each system. The systems were subjected to a set of subsequent 20 ps restrained minimizations, with the inner-bound ions restrained by 500 and solute restrained by 300, 100, 10, and 0 kcal mol^{-1} $Å^{-2}$ force constants, respectively. Then, the inner ions were relaxed during four-step energy minimizations (20 ps each) in which the force constant on channel ions was decreased to 300, 100, 10, and 0 kcal mol^{-1} $Å^{-2}$, respectively. The systems were then heated to 298 K over 50 ps at constant pressure with a force constant of 50 kcal mol^{-1} $Å^{-2}$ maintained for the solute and inner ions. These restraints were then scaled down in three stages (50 ps each) with the solute and inner ions restrained by 50 and 30 kcal mol^{-1} $Å^{-2}$ at the first step, 50 and 0 kcal mol^{-1} $Å^{-2}$ at the second step, and 30 and 0 kcal mol^{-1} $Å^{-2}$ at the final step. Eventually, the restraints were fully removed in the course of a 50 ps equilibration. Three different forms (NH_4^+, K^+, Na^+) of $[d(G_3T_4G_4)]_2$ were prepared in the same fashion. Separate 20 ns regular MD simulations were performed to examine the dynamics of different parts of $[d(G_3T_4G_4)]_2$. In some MD simulations, two bound ions were fixed at their binding sites inside of the channel using a harmonic potential (k = 100 kcal mol^{-1} $Å^{-2}$). The root-mean-square deviation (rmsd) calculations were performed with respect to the average structure. All MD simulations were performed in the isothermic−isobaric ensemble. Langevin dynamics and a Langevin piston algorithm were used to maintain the temperature at 298 K and 1 atm of pressure. The Particle Mesh Ewald (PME) method of calculating long-range electrostatic interactions was employed with a cutoff of 9 Å. Rattle was applied to constrain the bonds containing hydrogen atoms. A time step of 2 fs was used to integrate the equations of motion. All MD simulations were performed by using the program NAMD 2.7b3[61] and the CHARMM27 force field.[62,63] The program VMD 1.8.7 was used in the visualization and rmsd analysis.[64]

2.2. ABF MD Simulations. We have divided the reaction pathway along the $[d(G_3T_4G_4)]_2$ stem axis into four windows in a total length of approximately 28 Å. Two central windows, each being 4 Å long, were defined such that they include the upper and lower G-quartets, while the central G-quartet is covered by both windows. Two outer windows, each being 10 Å long, were defined to extend the reaction coordinate into edge-type and diagonal loops. The reaction coordinate for each window was defined along the central axis connecting the centers of mass of two consecutive G-quartets in the same window. This axis was dynamically updated during the ABF MD simulation. The vector between the ion and the midpoint of the axis was projected onto the axis and considered as the reaction coordinate. For all windows, a cylindrical confining potential (k = 100 kcal mol^{-1} $Å^{-2}$) was applied to restrict ion movement in the plane norm to the dynamic axis. Within each

dx.doi.org/10.1021/jp304760k | J. Phys. Chem. B 2012, 116, 9363−9370

window, the average force acting on the ion was accumulated in 0.1 Å sized bins. Application of ABFs was initiated after accumulation of 800 samples in individual bins. In some ABF MD simulations, harmonic restraints with a force constant of 3 kcal mol^{-1} Å^{-2} were applied to C1′ atoms of the guanine bases. Production runs in each window were typically continued for 3−6 ns. In order to obtain 2D potential of mean force (PMF) profiles, we performed ABF MD simulations along eight reaction pathways within the *XY* plane for a series of *Z* positions. The eight directions were (*X*,*Y*) = (1,0), (−1,0), (0,1), (0,−1), (1,1), (−1,1), (1,−1), and (−1,−1). A 2D PMF map was reconstructed from these 1D data.

3. RESULTS AND DISCUSSION

3.1. ABF MD Simulations. As we illustrated recently,[54] it is often useful to consider ion movement in a G-quadruplex DNA structure in two separate regions. One is within the G-quadruplex stem (or channel), and the other is from the stem entrance/exit point to bulk solution. In the discussion that follows, we treat these two regions separately. Figure 2 shows

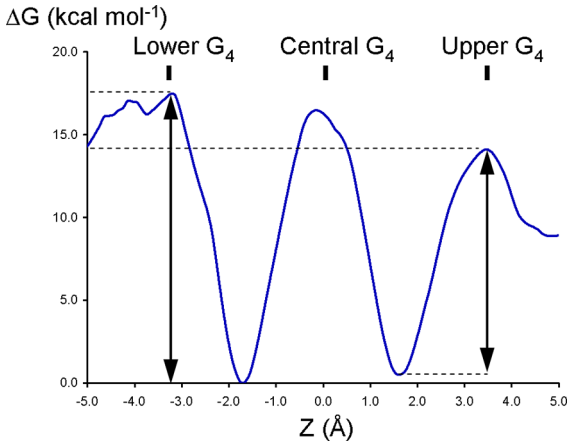

Figure 2. PMF profile for NH_4^+ ion movement inside of the $[d(G_3T_4G_4)]_2$ G-quadruplex stem.

the PMF profile for NH_4^+ ion movement within the $[d(G_3T_4G_4)]_2$ G-quadruplex stem obtained from "unconstrained" ABF MD simulations. Here, it is important to point out that in the unconstrained ABF MD simulation runs, while biasing forces are constantly being applied to the NH_4^+ ion, the G-quadruplex DNA structure itself is completely unconstrained (vide infra). As seen in Figure 2, the shape of the PMF profile is clearly asymmetrical. In particular, while the free-energy barrier for an exiting NH_4^+ ion to cross the upper G-quartet is approximately 14 kcal mol^{-1}, the corresponding barrier to cross the lower G-quartet is considerably higher, 17 kcal mol^{-1}. It is also important to note that the NH_4^+ ion movement between the two binding sites inside of the stem is also high, ∼17 kcal mol^{-1}. The PMF profile for K^+ ion movement within the $[d(G_3T_4G_4)]_2$ stem is similar to that seen for NH_4^+ (data given in the Supporting Information). In contrast, Na^+ ions can move through the G-quadruplex stem much more easily, experiencing free-energy barriers of only 5−7 kcal mol^{-1}; also see the Supporting Information. The observed similarity between NH_4^+ and K^+ and the discrepancy between NH_4^+/K^+ and Na^+ are in good agreement with our previous ABF MD results on a parallel-stranded $[d(TG_4T)]_4$ G-quadruplex.[54]

In the aforementioned ABF MD simulations, we found that the force converges rather rapidly. Typically, 1 ns ABF MD simulations can produce accurate PMF profiles for ion movement. We also noticed that in some cases, long ABF MD simulations (e.g., 10−20 ns) in fact produced erroneous results. The origin of the problem can be traced back to the fact that, in each ABF MD simulation run, we assumed single NH_4^+ ion occupancy inside of the G-quadruplex stem. If the NH_4^+ ion is kept in a particular region for a long period of time, the whole G-quadruplex structure may become unstable. This may be particularly true when we sample regions with steep free-energy features. To overcome this problem, in our previous study, we added weak constraints on C1′ atoms (a force constant of only 3 kcal mol^{-1} Å^{-2}) to prevent the G-quadruplex from falling apart in the absence of bound NH_4^+ ions.[54] Here, we refer these simulations as constrained ABF MD simulations. Our previous results showed that such weak constraints on C1′ atoms indeed do not significantly alter the free-energy barrier for an NH_4^+ ion to cross a G-quartet as C1′ atoms are somewhat remote from the center of a G-quartet and their movements are not strongly coupled to that of a guanine base. It is important to note that the assumption for single-ion occupancy in the $[d(G_3T_4G_4)]_2$ G-quadruplex stem is indeed a limitation of the present study. ABF MD simulations considering multiple ion occupancy are actively under investigation in this laboratory, and the results will be published elsewhere.

To further investigate the reproducibility of the unconstrained ABF MD results shown in Figure 2, we performed a complete set of constrained ABF MD simulations in which the four C1′ atoms in each G-quartet were confined by harmonic potentials with a weak force constant of 3 kcal mol^{-1} Å^{-2}, similar to what we did in the previous study.[54] The simulation results are summarized in Table 1. It is clear that the

Table 1. Free-Energy Barriers for NH_4^+ Ion Movement Inside of the $[d(G_3T_4G_4)]_2$ G-Quadruplex Stem Obtained from ABF MD Simulations under Various Conditions

	free-energy barrier (kcal mol^{-1})[a]		
constraint	lower G_4	central G_4	upper G_4
C1′ atoms on lower G_4	**20**	17	11
C1′ atoms on central G_4	17	**19**	15
C1′ atoms on upper G_4	16	16	**16**
none	17	17	14

[a]Boldface numbers highlight the energy barriers to cross the "constrained" G-quartets.

asymmetrical nature of the stem is also reflected in these constrained ABF MD simulations. For example, when the constraint is on the lower G-quartet, the barrier to cross the upper G-quartet is 11 kcal mol^{-1}. In comparison, when the constraint is on the upper G-quartet, the barrier to cross the lower G-quartet is 16 kcal mol^{-1}. It is also clear that, for each series of data shown in Table 1, the G-quartet on which the constraint is being applied exhibits the highest energy barrier. We also did the same constrained simulation test for the parallel-stranded $[d(TG_4T)]_4$ G-quadruplex. The results suggest that the NH_4^+ ion movement inside of the $[d(TG_4T)]_4$ stem is essentially symmetrical, with an average energy barrier of ∼14 kcal mol^{-1} (data given in the Supporting Information). This further proves that the asymmetry observed for NH_4^+ movement in $[d(G_3T_4G_4)]_2$ is real. A comparison between unconstrained and constrained ABF MD simulations for both

dx.doi.org/10.1021/jp304760k | J. Phys. Chem. B 2012, 116, 9363−9370

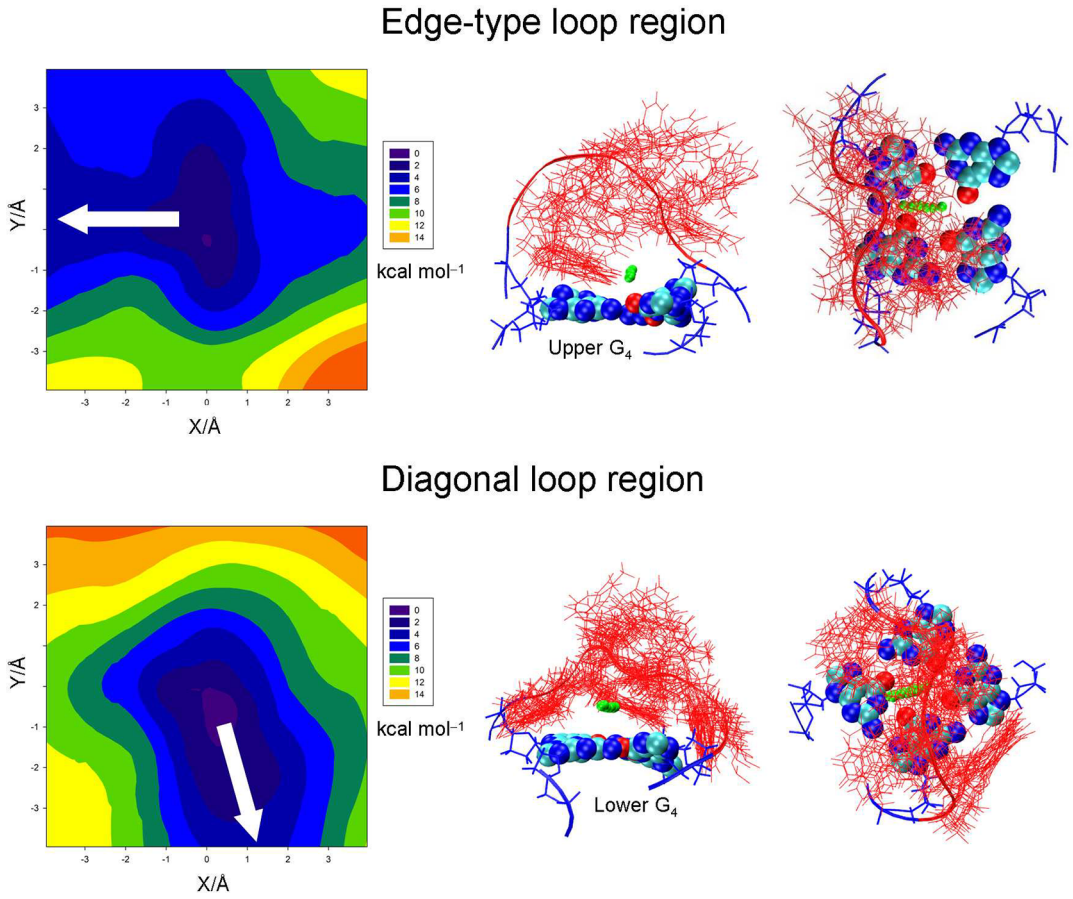

Figure 3. (left) 2D free-energy landscapes, (middle) side and (right) top views of the NH_4^+ ion movement in the edge-type and diagonal loop regions of the $[d(G_3T_4G_4)]_2$ G-quadruplex. The least-resistant pathway for "sideways" NH_4^+ ion movement is marked by an arrow in each 2D map and a string of green balls in the side and top views. In both side and top views, 20 simulation frames of the loop residues are shown to indicate the scope of loop movement.

G-quadruplex sequences leads to the following conclusions. First, the unconstrained ABF MD simulations yield reliable PMF profiles for ion movement in $[d(G_3T_4G_4)]_2$. Second, the weak constraint on C1′ atoms tends to increase the energy barrier of crossing the constrained G-quartet by 2−3 kcal mol^{-1} for NH_4^+ and K^+ ion movement but has negligible effects for Na^+ ion movement.

Once the NH_4^+ ion exits the G-quadruplex stem, its movement is no longer confined to the stem (channel) axis. As a result, it is necessary to consider its movement in all directions. In practice, we used ABF MD simulations to perform a 2D free-energy mapping in a plane perpendicular to the axis, that is, the *XY* plane. As seen from Figure 3, the 2D free-energy landscapes for NH_4^+ ion movement are rather flat as opposed to that seen inside of the stem shown in Figure 2. It is also important to note that, although the 2D maps look very different for the two ends, the actual free-energy costs for the NH_4^+ ion to reach bulk solution from the two-stem exit points are essentially the same, ∼2 kcal mol^{-1}. This is a somewhat surprising observation. A common argument found in the literature is that as the diagonal loop is "in the way" of ion passage to bulk solution, the energy barrier must be much higher for the NH_4^+ ion to exit the G-quadruplex stem from the end containing such a diagonal loop than that from the end containing other loops such as edge-type loops. The results shown in Figure 3 suggest a quite different picture. In fact, it appears that the NH_4^+ ion, once exiting the stem, can always find a "sideways" direction that imposes a minimum free-energy cost, regardless of the type of loop at the stem end. In other words, an exiting NH_4^+ ion does not need to get close to any loop. The loop topology determines only the direction at which the NH_4^+ ion travels toward bulk solution.

Now, we have generated a complete picture about NH_4^+ ion movement from its binding sites inside of the $[d(G_3T_4G_4)]_2$ G-quadruplex stem to bulk solution. By combining ABF MD simulation results shown in Figures 2 and 3, we can estimate the free-energy barriers for the lower and upper NH_4^+ ions to reach bulk solution to be 19 ± 1 and 16 ± 1 kcal mol^{-1}, respectively. Using the Eyring equation, we found the transport (exchange) rate to be 0.1 and 12 s^{-1} at 298 K for the lower and upper NH_4^+ ions, respectively. These estimates are in qualitative agreement with the experimental results reported by Šket and Plavec for the same G-quadruplex sequence.[13]

3.2. Regular MD Simulations. To supplement the aforementioned ABF MD simulations, we performed a regular 20 ns, unconstrained MD simulation to further monitor the NH_4^+ ion movement in the $[d(G_3T_4G_4)]_2$ G-quadruplex structure. Figure 4 shows several snap shots of the simulation trajectories. Initially, the two bound NH_4^+ ions are in their equilibrium positions within the quadruplex stem, each being sandwiched between two G-quartets. The simulation shows that while the upper NH_4^+ ion very quickly (in approximately 100 ps) exits the stem by passing through the upper G-quartet, the lower NH_4^+ ion remains at the binding site for as long as 8

dx.doi.org/10.1021/jp304760k | J. Phys. Chem. B 2012, 116, 9363−9370

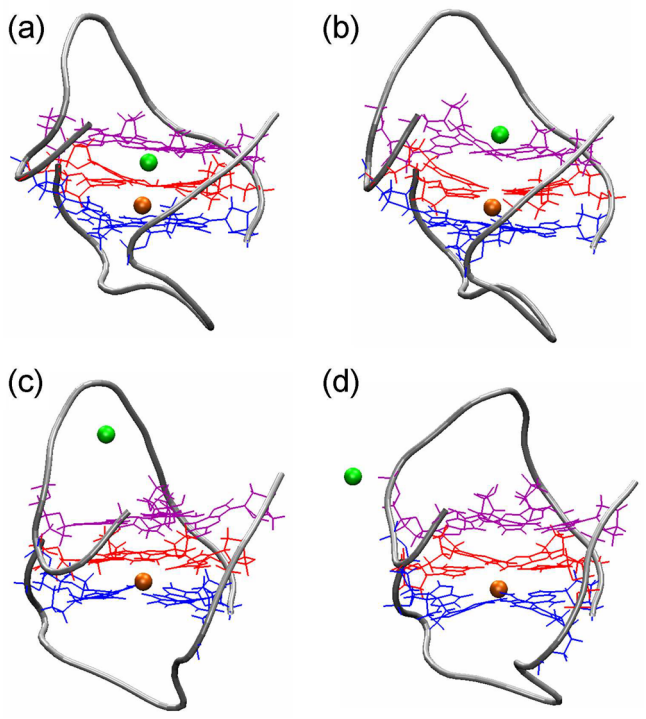

Figure 4. Representative frames from a 20 ns unconstrained MD simulation run for the $[d(G_3T_4G_4)]_2$ G-quadruplex. Initially, two bound NH_4^+ ions are inside of the quadruplex stem. (a) < 100 ps, (b) 100−700 ps, (c) 700 ps−4.9 ns, and (d) 4.9−8.2 ns. For clarity, two different colors are used to distinguish the two NH_4^+ ions.

ns. During this entire period of 8 ns, we did not observe re-entry of the upper NH_4^+ ion back to the stem. In the end, the lower NH_4^+ ion exits the stem through the lower G-quartet, and the whole G-quadruplex structure becomes unstable (data not shown). Remarkably, during the entire period of 8 ns before the lower NH_4^+ exits the stem, it never once crosses the central G-quartet. This indicates that the energy barrier to cross the central G-quartet is prohibitively high, which is consistent with the ABF MD simulation results discussed earlier. In this context, ion movement between two adjacent sites within a G-quadruplex stem has been seen in previous MD simulations.[36,40,42,65] More recently, Golovin and co-workers[66] even observed a concerted ion movement in which a free ion from bulk solution enters the G-quadruplex stem from one side while simultaneously expelling the bound ion into bulk solution from the other side. Although caution must be exercised to avoid overinterpretation of the regular MD simulation results, we believe that the observed contrast in ion movement between the two bound NH_4^+ ions within the aforementioned 20 ns MD simulation does provide additional support for the free-energy results obtained from ABF MD simulations.

To further investigate whether the rigidity of a G-quartet is, in any way, related to its overall structural dynamics, we performed another 20 ns regular MD simulation in which the two bound NH_4^+ ions were fixed at their equilibrium binding sites inside of the $[d(G_3T_4G_4)]_2$ G-quadruplex stem. This simulation allows us to analyze dynamics for different parts of the G-quadruplex structure, including the stem backbone and diagonal and edge-type loops. Figure 5 displays the rmsd analysis of this simulation run. It is seen that with two bound NH_4^+ ions in place, the whole G-quadruplex structure is very stable. Several observations are worth mentioning. First, the two end G-quartets are less stable (showing larger fluctuations) than the central one. This is probably due to the fact that while each of the end G-quartets interacts with only one bound NH_4^+ ion, the central G-quartet is stabilized simultaneously by both NH_4^+ ions. Second, the stem backbone is also very stable. Third, the diagonal loop is the most flexible.

3.3. Stiffness of a G-Quartet Determined by Base Stacking: A Hypothesis. Although our ABF MD simulations have reproduced reasonably well the experimental results, they do not automatically point to the structural factor that determines the various free-energy barriers for NH_4^+ ion movement. One can imagine that the energy barrier for an NH_4^+ ion to pass through a G-quartet inside of a G-quadruplex stem must be related to the stiffness or flexibility of that G-quartet. This is because the G-quartet in question must open, at least partially, in order to allow an NH_4^+ ion to pass through, and the opening of a G-quartet would destroy partially the base stacking. Therefore, a rigid G-quartet must impose a high energy barrier for a passing NH_4^+ ion, whereas a dynamical or flexible G-quartet should be less difficult to move through. For the G-quartet inside of a G-quadruplex stem, its stiffness or flexibility appears to be dominated by the base stacking interactions between the G-quartet in question and adjacent G-quartets. Here, we hypothesize that inside of a G-quadruplex stem, the base stacking arrangement around a particular G-quartet determines its stiffness or flexibility. Of course, for a G-quartet appearing at the end of a G-quadruplex stem, base stacking from loop residues, if any, may also contribute to its stiffness. In fact, Plavec and co-workers[15] have previously noticed that the base stacking between end G-quartets and loop thymine bases significantly slows down the NH_4^+ exiting rate in $[d(G_4T_3G_4)]_2$ (vide infra).

Now, let us examine base stacking interactions inside of a G-quadruplex stem. As Webba da Silva pointed out,[67] there are four possible types of intrastrand base stacking according to the glycosidic bond angle (GBA) propagation along the 5′ → 3′ direction, 5′-syn−anti, 5′-syn−syn, 5′-anti−syn, and 5′-anti−anti. Recently, Cang et al.[68] performed free-energy calculations that show the following relative stability trend for these four types of base stacking, syn−anti > anti−anti > anti−syn > syn−syn. As base stacking between G-quartets gets amplified at least four times, the stabilization effect from base stacking can be quite significant. For example, according to the computational results reported by Cang et al.,[68] a G-quartet in the syn−anti stacking mode may be more stable than one in the anti−anti stacking mode by as large as 16 kcal mol^{-1}. Close inspection of the $[d(G_3T_4G_4)]_2$ structure (PDB code 1U64)[12] reveals that while the base stacking between the upper and central G-quartets is of the anti−anti type, the lower and central G-quartets are in the syn−anti base stacking mode, as illustrated in Figure 6. These two different types of base stacking arrangement in $[d(G_3T_4G_4)]_2$ have been noticed previously.[69] In the syn−anti base stacking mode, the five-membered rings from two adjacent guanine bases are nearly perfectly on top of one another, allowing very sufficient base stacking. In contrast, the two guanine bases are offset in the anti−anti base stacking mode. This immediately suggests that the lower G-quartet must be more rigid than the upper G-quartet. This prediction is in full agreement with both the ABF MD simulation and experimental results. Our hypothesis offers an explanation as to why the NH_4^+ ion movement in the $[d(G_3T_4G_4)]_2$ G-quadruplex stem exhibits a directional asymmetry. Furthermore, several other experimental observations seem to support

dx.doi.org/10.1021/jp304760k | J. Phys. Chem. B 2012, 116, 9363−9370

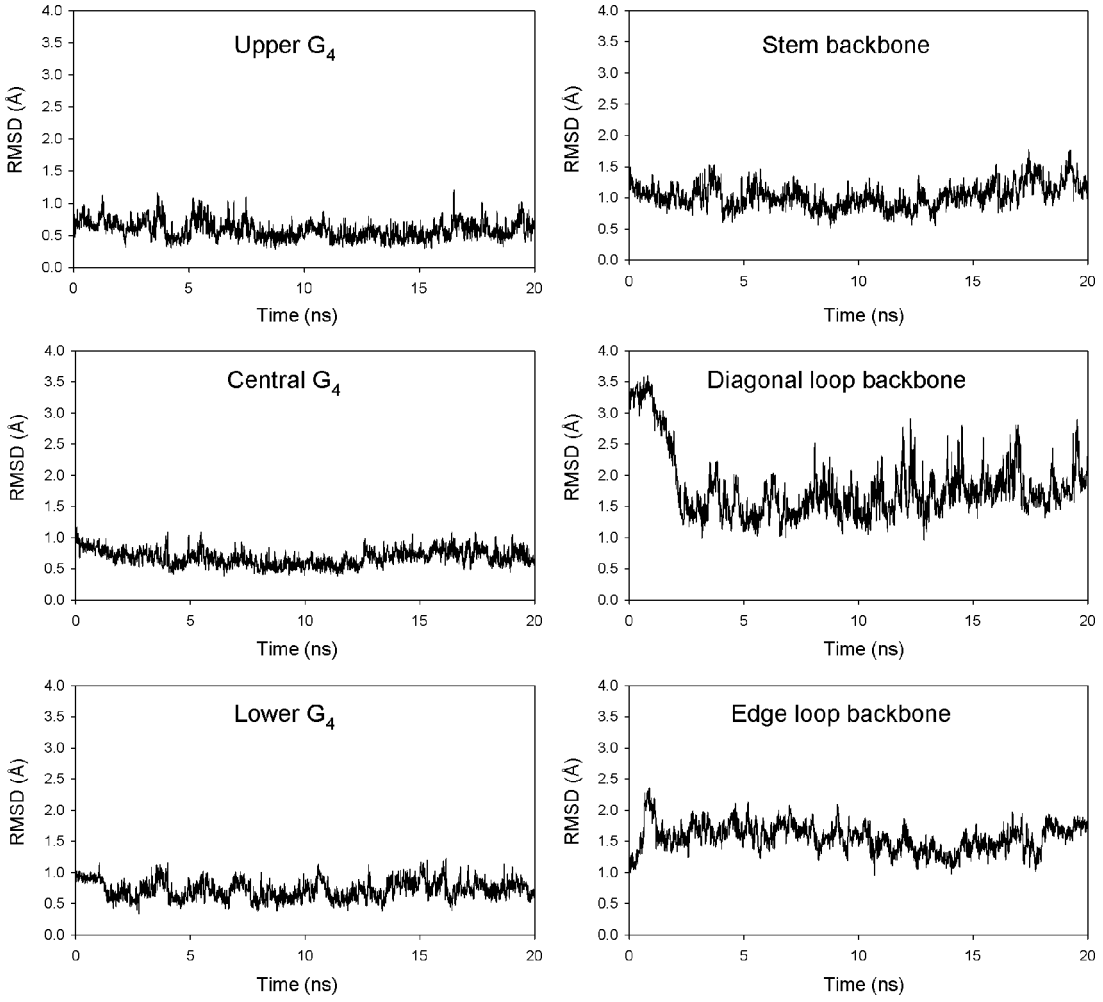

Figure 5. The rmsd results for different parts of the $[d(G_3T_4G_4)]_2$ G-quadruplex during a 20 ns regular MD simulation run in which the two bound NH_4^+ ions are constrained at their binding sites.

our hypothesis. First, the NH_4^+ ion movement in the parallel-stranded $[d(TG_4T)]_4$ quadruplex stem appears to exhibit the fastest transport rates,[16] and the NH_4^+ ion movement is symmetrical, as we discussed earlier. This is because all G-quartets in $[d(TG_4T)]_4$ are involved in the anti−anti base stacking.[70,71] Second, the NH_4^+ ion movement in the unimolecular $[d(G_4(T_4G_4)_3)]$ G-quadruplex stem is rather slow.[14] This is because the GBA propagation for the stem is 5′-syn−anti−syn−anti, which makes both end G-quartets very rigid. Third, Plavec and co-workers[15] reported that the NH_4^+ ion movement throughout the antiparallel $[d(G_4T_3G_4)]_2$ G-quadruplex stem is too slow to be reliably detected. In this particular G-quadruplex structure, the two end G-quartets not only are involved in the most stable syn−anti stacking from inner G-quartets but also participate in significant base stacking from the edge-type T_3 loops. This latter aspect was also noticed by Plavec and co-workers,[15] as mentioned earlier. As a result, the two very stiff end G-quartets slow down the NH_4^+ ion flow throughout the G-quadruplex stem.

Our hypothesis not only provides new insights into the structural factor that controls ion movement in G-quadruplexes but also offers a guideline for the design of G-quadruplex ion channels. For example, the hypothesis predicts that those G-quadruplexes with all G-quartets being in the anti−anti stacking mode likely exhibit ion channel behaviors. As mentioned earlier, this GBA arrangement occurs in the parallel-stranded $[d(TG_4T)]_4$. The same anti−anti base stacking is also seen in the crystal structure of the K^+ form of four repeat human telomeric DNA $d(AG_3(T_2AG_3)_3)$.[72] We should emphasize, however, that our hypothesis about G-quartet stiffness is perhaps only valid in the context of movement of large ions such as NH_4^+ and K^+. For Na^+, it is not clear whether base stacking interactions would make a significant contribution to the energy barrier for ion passage. The currently available experimental and computational data appear to suggest that Na^+ ions pass through all G-quadruplex channels with essentially the same free-energy barrier of ∼5 kcal mol^{-1}. This also suggests that while some G-quadruplex structures may not be channel-like for NH_4^+ and K^+ ions, they always allow Na^+ ions to pass through with ease.

4. CONCLUSIONS

In this study, we have performed extensive ABF and regular MD simulations to obtain information about the energetics of NH_4^+ ion movement in the $[d(G_3T_4G_4)]_2$ G-quadruplex. We found that the free-energy barriers for a bound NH_4^+ ion to exit from the two ends of the $[d(G_3T_4G_4)]_2$ G-quadruplex stem differ by 3−4 kcal mol^{-1}, which corresponds to approximately a factor of 10−100 in transport rates at 298 K. These computational results are in qualitative agreement with the

dx.doi.org/10.1021/jp304760k | J. Phys. Chem. B 2012, 116, 9363−9370

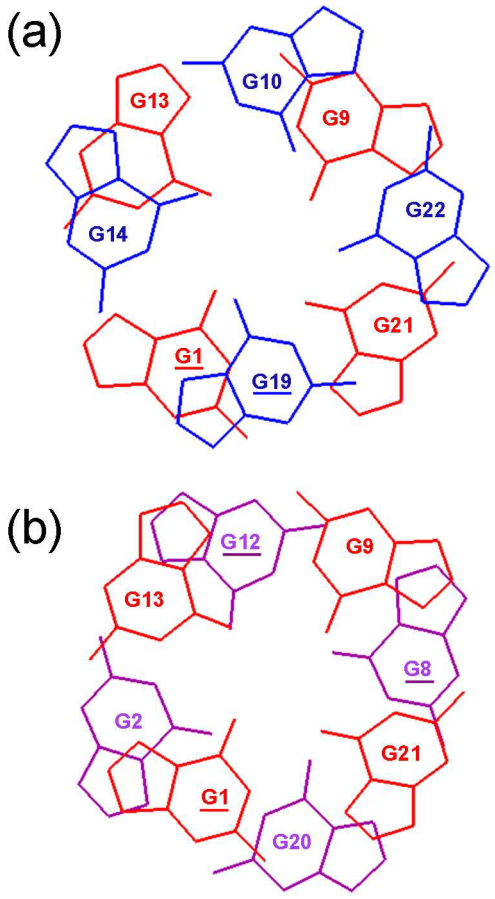

Figure 6. Base stacking between (a) upper (in blue) and central (in red) G-quartets and (b) lower (in purple) and central (in red) G-quartets in the $[d(G_3T_4G_4)]_2$ G-quadruplex stem (PDB code: 1U64).[12] The underlying residues are in syn conformation.

experimental results. The simulations also confirm that the free-energy barrier to cross the central G-quartet is also high. The 2D free-energy maps suggest that once the NH_4^+ ion exits the G-quadruplex stem, it faces a very shallow free-energy landscape that allows it to easily reach bulk solution, regardless of the actual loop topology at the end. We further hypothesize that the stiffness of a G-quartet is primarily determined by the base stacking interactions around it. Therefore, the stiffness of a G-quartet should follow the known relative stability trend for base stacking, syn−anti > anti−anti > anti−syn > syn−syn. For a G-quartet inside of the quadruplex stem, base stacking interactions from adjacent G-quartets are important. For an end G-quartet, one should consider base stacking from both the inner G-quartet and possibly loop residues. This hypothesis seems to be consistent with currently available dynamical information about ion movement within G-quadruplex DNA structures. More quantitative evaluation of G-quartet stiffness and its relationship to free-energy barriers for ion passage is underway in this laboratory.

■ ASSOCIATED CONTENT

Supporting Information

PMF profiles for K^+ and Na^+ ion movement inside of the $[d(G_3T_4G_4)]_2$ G-quadruplex stem. Free-energy barriers for NH_4^+ ion movement in a parallel-stranded $[d(TG_4T)]_4$ G-quadruplex obtained under various conditions. This material is available free of charge via the Internet at http://pubs.acs.org.

■ AUTHOR INFORMATION

Corresponding Author

*E-mail: gang.wu@chem.queensu.ca.

Notes

The authors declare no competing financial interest.

■ ACKNOWLEDGMENTS

This work was supported by the Natural Sciences and Engineering Research Council (NSERC) of Canada. All MD simulations were performed on the SHARCNET. We are grateful to Professor Nick Mosey for assistance and helpful discussion and anonymous referees for helpful suggestions.

■ REFERENCES

(1) Neidle, S.; Parkinson, G. N. *Curr. Opin. Struct. Biol.* **2003**, *13*, 275−283.
(2) Davis, J. T. *Angew. Chem., Int. Ed.* **2004**, *43*, 668−698.
(3) Hud, N. V.; Plavec, J. In *Quadruplex Nucleic Acids*; Neidle, S., Balasubramanian, S., Eds.; The Royal Society of Chemistry: Cambridge, U.K., 2006; pp 100−130.
(4) Engelhart, A. E.; Plavec, J.; Persil, Ö.; Hud, N. V. In *Nucleic Acid−Metal Ion Interactions*; Hud, N. V., Ed.; RSC Publishing: London, 2009; pp 118−153.
(5) Hud, N. V.; Smith, F. W.; Anet, F. A. L.; Feigon, J. *Biochemistry* **1996**, *35*, 15383−15390.
(6) Forman, S. L.; Fettinger, J. C.; Pieraccini, S.; Gottarelli, G.; Davis, J. T. *J. Am. Chem. Soc.* **2000**, *122*, 4060−4067.
(7) Kaucher, M. S.; Harrell, W. A.; Davis, J. T. *J. Am. Chem. Soc.* **2006**, *128*, 38−39.
(8) Hud, N. V.; Schultze, P.; Feigon, J. *J. Am. Chem. Soc.* **1998**, *120*, 6403−6404.
(9) Hud, N. V.; Schultze, P.; Sklenar, V.; Feigon, J. *J. Mol. Biol.* **1999**, *285*, 233−243.
(10) Feigon, J.; Butcher, S. E.; Finger, L. D.; Hud, N. V. *Methods Enzymol.* **2001**, *338*, 400−420.
(11) Šket, P.; Črnugelj, M.; Kozminski, W.; Plavec, J. *Org. Biomol. Chem.* **2004**, *2*, 1970−1973.
(12) Šket, P.; Črnugelj, M.; Plavec, J. *Nucleic Acids Res.* **2005**, *33*, 3691−3697.
(13) Šket, P.; Plavec, J. *J. Am. Chem. Soc.* **2007**, *129*, 8794−8800.
(14) Podbevšek, P.; Hud, N. V.; Plavec, J. *Nucleic Acids Res.* **2007**, *35*, 2554−2563.
(15) Podbevšek, P.; Šket, P.; Plavec, J. *J. Am. Chem. Soc.* **2008**, *130*, 14287−14293.
(16) Šket, P.; Plavec, J. *J. Am. Chem. Soc.* **2010**, *132*, 12724−12732.
(17) Zavasnik, J.; Podbevšek, P.; Plavec, J. *Biochemistry* **2011**, *50*, 4155−4161.
(18) Rovnyak, D.; Baldus, M.; Wu, G.; Hud, N. V.; Feigon, J.; Griffin, R. G. *J. Am. Chem. Soc.* **2000**, *122*, 11423−11429.
(19) Wu, G.; Wong, A. *Chem. Commun.* **2001**, 2658−2659.
(20) Wong, A.; Fettinger, J. C.; Forman, S. L.; Davis, J. T.; Wu, G. *J. Am. Chem. Soc.* **2002**, *124*, 742−743.
(21) Wu, G.; Wong, A.; Gan, Z. H.; Davis, J. T. *J. Am. Chem. Soc.* **2003**, *125*, 7182−7183.
(22) Wong, A.; Wu, G. *J. Am. Chem. Soc.* **2003**, *125*, 13895−13905.
(23) Wu, G.; Wong, A. *Biochem. Biophys. Res. Commun.* **2004**, *323*, 1139−1144.
(24) Ida, R.; Wu, G. *Chem. Commun.* **2005**, 4294−4296.
(25) Wu, G.; Gan, Z.; Kwan, I. C. M.; Fettinger, J. C.; Davis, J. T. *J. Am. Chem. Soc.* **2011**, *133*, 19570−19573.
(26) Xu, Q. W.; Deng, H.; Braunlin, W. H. *Biochemistry* **1993**, *32*, 13130−13137.
(27) Deng, H.; Braunlin, W. H. *J. Mol. Biol.* **1996**, *255*, 476−483.
(28) Wong, A.; Ida, R.; Wu, G. *Biochem. Biophys. Res. Commun.* **2005**, *337*, 363−366.
(29) Ida, R.; Wu, G. *J. Am. Chem. Soc.* **2008**, *130*, 3590−3602.
(30) Snoussi, K.; Halle, B. *Biochemistry* **2008**, *47*, 12219−12229.

(31) Basu, S.; Szewczak, A. A.; Cocco, M.; Strobel, S. A. *J. Am. Chem. Soc.* **2000**, *122*, 3240−3241.
(32) Gill, M. L.; Strobel, S. A.; Loria, J. P. *J. Am. Chem. Soc.* **2005**, *127*, 16723−16732.
(33) Kwan, I. C. M.; Wong, A.; She, Y.-M.; Smith, M. E.; Wu, G. *Chem. Commun.* **2008**, 682−684.
(34) Ross, W. S.; Hardin, C. C. *J. Am. Chem. Soc.* **1994**, *116*, 6070−6080.
(35) Strahan, G. D.; Keniry, M. A.; Shafer, R. H. *Biophys. J.* **1998**, *75*, 968−981.
(36) Špačková, N.; Berger, I.; Šponer, J. *J. Am. Chem. Soc.* **1999**, *121*, 5519−5534.
(37) Read, M. A.; Neidle, S. *Biochemistry* **2000**, *39*, 13422−13432.
(38) Špačková, N.; Berger, I.; Šponer, J. *J. Am. Chem. Soc.* **2001**, *123*, 3295−3307.
(39) Fadrná, E.; Špačková, N.; Štefl, R.; Koča, J.; Cheatham, T. E., 3rd; Šponer, J. *Biophys. J.* **2004**, *87*, 227−242.
(40) Chowdhury, S.; Bansal, M. *J. Phys. Chem. B* **2001**, *105*, 7572−7578.
(41) Cavallari, M.; Calzolari, A.; Garbesi, A.; Di Felice, R. *J. Phys. Chem. B* **2006**, *110*, 26337−26348.
(42) Šponer, J; Špačková, N. *Methods* **2007**, *43*, 278−290.
(43) Haider, S.; Parkinson, G. N.; Neidle, S. *Biophys. J.* **2008**, *95*, 296−311.
(44) Pagano, B.; Mattia, C. A.; Cavallo, L.; Uesugi, S.; Giancola, C.; Fraternali, F. *J. Phys. Chem. B* **2008**, *112*, 12115−12123.
(45) Li, M.-H.; Luo, Q.; Xue, X.-G.; Li, Z.-S. *J. Mol. Struct.: THEOCHEM* **2010**, *952*, 96−102.
(46) Gu, J.; Leszczynski, J. *J. Phys. Chem. A* **2000**, *104*, 6308−6313.
(47) Gu, J.; Leszczynski, J. *J. Phys. Chem. A* **2002**, *106*, 529−532.
(48) Meyer, M.; Brandl, M.; Suhnel, J. *J. Phys. Chem. A* **2001**, *105*, 8223−8225.
(49) Meyer, M.; Steinke, T.; Brandl, M.; Suhnel, J. *J. Comput. Chem.* **2001**, *22*, 109−124.
(50) van Mourik, T.; Dingley, A. J. *Chem.—Eur. J.* **2005**, *11*, 6064−6079.
(51) van der Wijst, T.; Fonseca Guerra, C.; Swart, M.; Bickelhaupt, F. M.; Lippert, B. *Angew. Chem., Int. Ed.* **2009**, *48*, 3285−3287.
(52) Fonseca Guerra, C.; Zijlstra, H.; Paragi, G.; Bicklhaupt, F. M. *Chem.—Eur. J.* **2011**, *17*, 12612−12622.
(53) Jissy, A. K.; Ashik, U. P. M.; Datta, A. *J. Phys. Chem. C* **2011**, *115*, 12530−12546.
(54) Akhshi, P.; Mosey, N. J.; Wu, G. *Angew. Chem., Int. Ed.* **2012**, *51*, 2850−2854.
(55) Darve, E.; Pohorille, A. *J. Chem. Phys.* **2001**, *115*, 9169−9183.
(56) Rodríguez-Gómez, D.; Darve, E.; Pohorille, A. *J. Chem. Phys.* **2004**, *120*, 3563−3578.
(57) Darve, E.; Rodríguez-Gómez, D.; Pohorille, A. *J. Chem. Phys.* **2008**, *128*, 144120.
(58) Hénin, J.; Chipot, C. *J. Chem. Phys.* **2004**, *121*, 2904−2914.
(59) Chipot, C.; Hénin, J. *J. Chem. Phys.* **2005**, *123*, 244906.
(60) Hénin, J.; Fiorin, J.; Chipot, C.; Klein, M. L. *J. Chem. Theory Comput.* **2010**, *6*, 35−47.
(61) Phillips, J. C.; Braun, R.; Wang, W.; Gumbart, J.; Tajkhorshid, E.; Villa, E.; Chipot, C.; Skeel, R. D.; Kalé, L.; Schulten, K. *J. Comput. Chem.* **2005**, *26*, 1781−1802.
(62) Foloppe, N.; MacKerell, A. D., Jr. *J. Comput. Chem.* **2000**, *21*, 86−104.
(63) MacKerell, A. D., Jr.; Banavali, N. K. *J. Comput. Chem.* **2000**, *21*, 105−120.
(64) Humphrey, W.; Dalke, A.; Schulten, K. *J. Mol. Graphics* **1996**, *14.1*, 33−38.
(65) Stefl, R.; Cheatham, T. E., 3rd; Spackova, N.; Fadrna, E.; Berger, I.; Koca, J.; Sponer, J. *Biophys. J.* **2003**, *85*, 1787−1804.
(66) Reshetnikov, R. V.; Sponer, J.; Rassokhina, O. I.; Kopylov, A. M.; Tsvetkov, P. O.; Makarov, A. A.; Golovin, A. V. *Nucleic Acids Res.* **2011**, *39*, 9789−9802.
(67) Webba da Silva, M. *Chem.—Eur. J.* **2007**, *13*, 9738−9745.
(68) Cang, X.; Sponer, J.; Cheeatham, T. E., III. *Nucleic Acids Res.* **2011**, *39*, 4499−4512.
(69) Šket, P.; Črnugelj, M.; Plavec, J. *Bioorg. Med. Chem.* **2004**, *12*, 5735−5744.
(70) Laughlan, G.; Murchie, A. I. H.; Norman, D. G.; Moore, M. H.; Moody, P. C. E.; Lilley, D. M. J.; Luisi, B. *Science* **1994**, *265*, 520−524.
(71) Phillips, K.; Dauter, Z.; Murchie, A. I. H.; Lilley, D. M. J.; Luisi, B. *J. Mol. Biol.* **1997**, *273*, 171−182.
(72) Parkinson, G. N.; Lee, M. P. H.; Neidle, S. *Nature* **2002**, *417*, 876−880.